Supporting Information for Sub-mesoscale Wind-Front Interactions: the combined impact of thermal and current feedback

Yue Bai [1], Andrew F. Thompson [1], Ana B. Villas Bôas[2], Patrice Klein[1,3],

Hector S. Torres[3], Dimitris Menemenlis[3]

[1]California Institute of Technology

[2]Colorado School of Mines

[3]Jet Propulsion Laboratory

Contents

Introduction

This supplementary information provides additional panels and error analysis of 2-D conditional mean plots in the energetic subdomain in Drake Passage. Specifically, this document shows a wind stress divergence reconstruction as a function of surface divergence

and downwind SST gradient. Also, a discussion of the spatial distribution of the feedback coefficients, which is not included in the main text, is provided here. Finally, we compare our analysis in the energetic region of the Southern Ocean to a more quiescent subdomain (Fig. 1).

Additional 2-D conditional mean plots and associated error analysis

Considering wind stress curl and divergence as a function of both surface ocean vorticity/divergence and crosswind/downwind SST gradients, there are eight combinations of 2-D conditional mean plots to visualize the impact of TFB and CFB on spatial wind stress patterns (four for each of wind stress curl and divergence). Four of these figures are shown in the panels of Fig. 2, which highlight both the interaction between TFB and CFB (Fig. 2 a,d) and 1-D scenarios where only TFB is significant (Fig. 2 b,c). The other four combinations are computed and averaged in the same way as in the main text (Fig. 2), and showcase scenarios where only components of the CFB are relevant to the selected wind stress product (Fig. S1 b,c), or when both chosen components of TFB and CFB are irrelevant (Fig. S1 a,d). To illustrate, in Fig. S1 b, the mean wind stress curl is close to zero when the ocean surface vorticity is weak, regardless of the magnitude of the downwind SST gradient. Positive wind stress curl values occur in the negative vorticity regime. This shows that ocean surface currents and the CFB set small-scale variability in wind stress curl, while downwind SST gradient plays a negligible role here. This CFB control is also visible in Fig. S1 c, in which ocean surface divergence is negatively correlated with wind stress divergence. In Fig. S1 a,d, in which both ocean vorticity/divergence and cross/downwind SST gradients considered are uncorrelated with the wind stress fields, the distributions are random and no clear zero-lines are visible. Similar to the properties

discussed in the main text, there is an asymmetric distribution of vorticity with regions having a Rossby number larger than 1 preferentially associated with cyclonic vorticity

Assessment of errors associated with the 2-D conditional mean calculation is needed to provide confidence in our documented patterns of TFB and CFB, especially for large values of vorticity/divergence and strong SST gradients. The total number of data points within ± 1 standard deviation of the bin-averaged value (for each bin, Fig. 2) is shown in Fig. S2. As expected, most data points occur at small vorticity/divergence and SST gradient values. However, there are substantial data points at the extremes to provide meaningful statistics. Standard errors (Fig. S3) $\frac{\sigma}{\sqrt{n}}$, in which σ is the standard deviation and n is the total number of points in each bin, are computed to highlight the credibility of the mean values in each bin. Bins with higher standard error values are generally located at the edge of the distributions and might indicate a regions of parameter space with insufficient data or a greater impact of outliers.

Wind stress divergence reconstruction

Following the same method of producing a linear 2-Dreconstruction of wind stress curl in Sec. 3, here we present the reconstruction method for wind stress divergence:

$$\boldsymbol{\nabla} \cdot \boldsymbol{\tau} = \alpha \boldsymbol{\delta}/|f| + \beta \boldsymbol{\nabla}_d \mathrm{SST}, \tag{1}$$

where α is still the coefficient of CFB, but for ocean surface divergence $\boldsymbol{\delta}/|f|$, and β for downwind SST gradient $\boldsymbol{\nabla}_d$SST. 2-D and 1-D calculations remain the same as in Sec. 3.

In the energetic subdomain, most variance in wind stress divergence (Fig. S4) is explained by variability in the downwind SST gradient, even though surface ocean divergence has a similar order of magnitude as vorticity at the nominal resolution of this simulation,

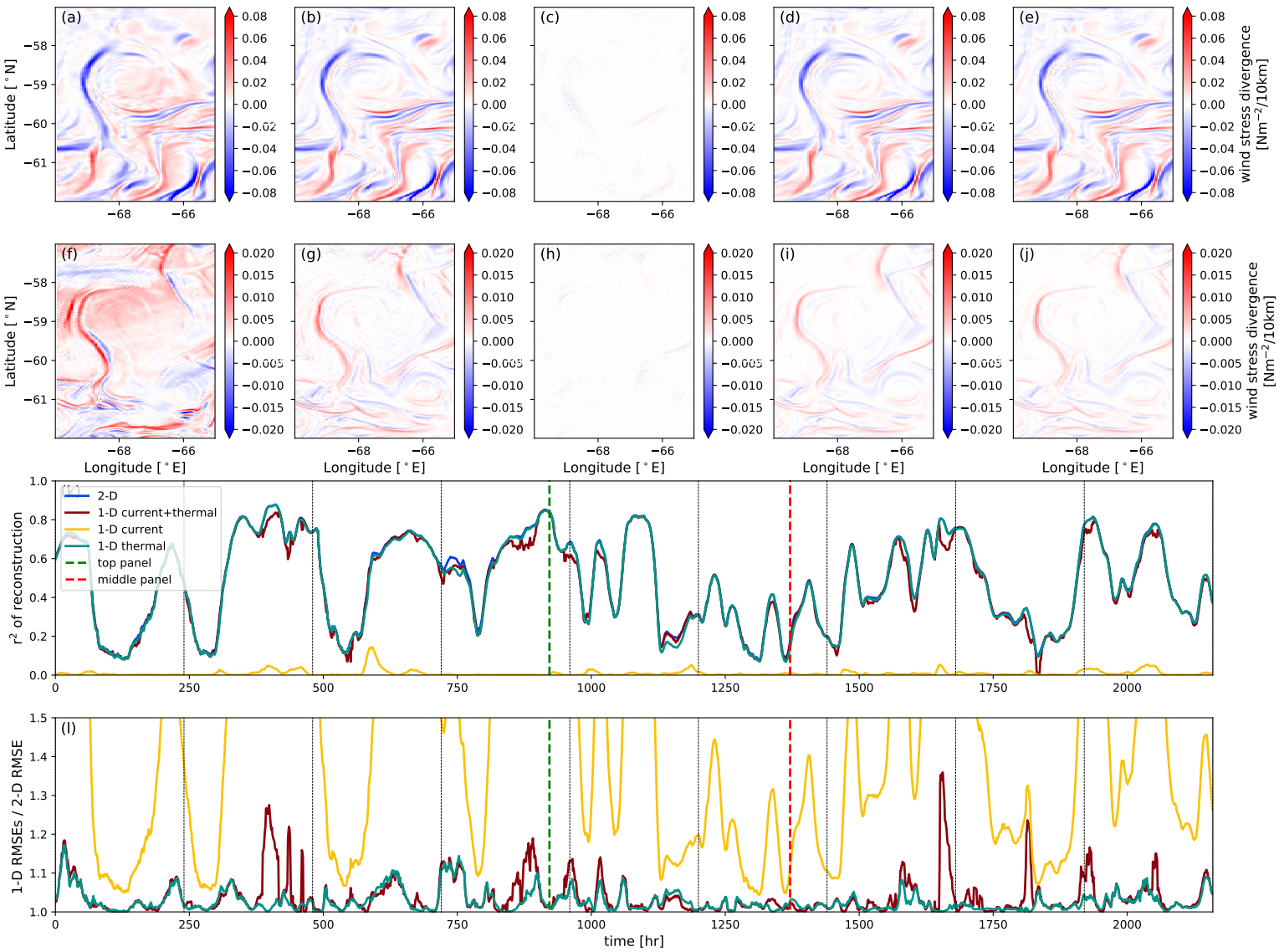

Figure S4. Wind stress divergence reconstruction. The top two panels are taken at the same snapshot as the wind stress curl reconstruction (Fig. 3). Within the top two panels, from left to right are simulated wind stress curl (a,f), 2-D reconstruction (b,g), 1-D current reconstruction (c,h), 1-D thermal (d,i), and 1-D current + thermal (e,j).

$\sim$10 km. Unlike for wind stress curl, for most times, 1-D thermal reconstruction captures the structure of wind stress divergence as well as the dependent 2-D or independent 1-D current + thermal reconstruction. This suggests that wind stress divergence is dominated by mesoscale oceanic variability; at these scales, the ocean surface divergence is negligible. Overall, the 1-D thermal reconstruction has 0-17% larger RMSE than the 2-D reconstruction; averaged over time, the error associated with the 1-D thermal reconstruction is 3% larger. It is anticipated that, with increased spatial resolution and improved representation of submesoscale features, the impact of ocean surface divergence on the wind stress field will enhance. At these smaller scales, consideration of ocean surface divergence when reconstructing submesoscale wind stress divergence will be necessary.

Spatial distribution of α and β with surface dynamical features and implications for future observational missions

As mentioned briefly in the main text, the coefficients of TFB and CFB contributions to the wind stress curl (β and α, respectively) are spatially variable, and the patterns of variability relate to coherent structures in the upper ocean. Both α and β, as well as the magnitude of the Pearson correlation coefficient r^2 determined from the 2-D reconstructed and simulated wind stress curl (Fig. 3), are sensitive to dynamical regimes identified from an Okubo-Weiss (OW) filter. Positive values of OW indicate a strain-dominated region and negative values of OW indicate a vorticity-dominated region. Following a similar approach based on the strain-vorticity joint probability distribution functions in Balwada, Xiao, Smith, Abernathey, and Gray (2021), the coefficient calculations (Sec. 3) are repeated using a subset of wind and ocean data in the energetic subdomain, screening with the OW parameter. One- and fifteen-day time-averaging windows are used as in the

main text. When conditioning on $OW/f^2 < 0$ (Fig. S5), β has minimal fluctuations at daily time scales, and α increases by 11% on average. However, when conditioning on areas with $OW/f^2 > 0.2$ (Fig. S6), daily calculated α and r^2 are enhanced by 36% and 30%, respectively.

These changes in the correlation coefficients based on OW conditions suggest that the intensity of wind-front interactions is visibly strengthened in filamentary strain regions as compared to the center of eddies. Yet, the estimates of coefficients in eddy centers are more representative of subdomain-averaged values (Fig. S5). In future observational campaigns, such as S-MODE(Farrar et al., 2020), estimation of domain-averaged wind-front interactions would require broad spatial measurements of surface velocity and temperature, covering multiple mesoscale and submesoscale eddies. More localized quantification of enhanced sub-mesoscale wind-front interaction requires persistent and collocated sampling in narrow filamentary structures. At the same time, in-situ Lagrangian measurements, such as surface drifters, have the propensity to converge at frontal regions, and therefore are subject to potentially misrepresenting and biasing estimations on average wind-front interaction intensity in the domain.

Analyses in the quiescent region

In the quiescent region of the Southern Ocean considered in this study (Fig. 1, left box), the same analyses of the 2-D conditional mean (Fig. 2), wind stress curl reconstruction (Fig. 3), and temporal coefficient variability (Fig. 4) are conducted and shown here for comparison. Overall, despite differences in the surface Ro distributions (Fig. 1 c,d), background energy levels (Fig. 1 a), and the range of SST gradients between the two

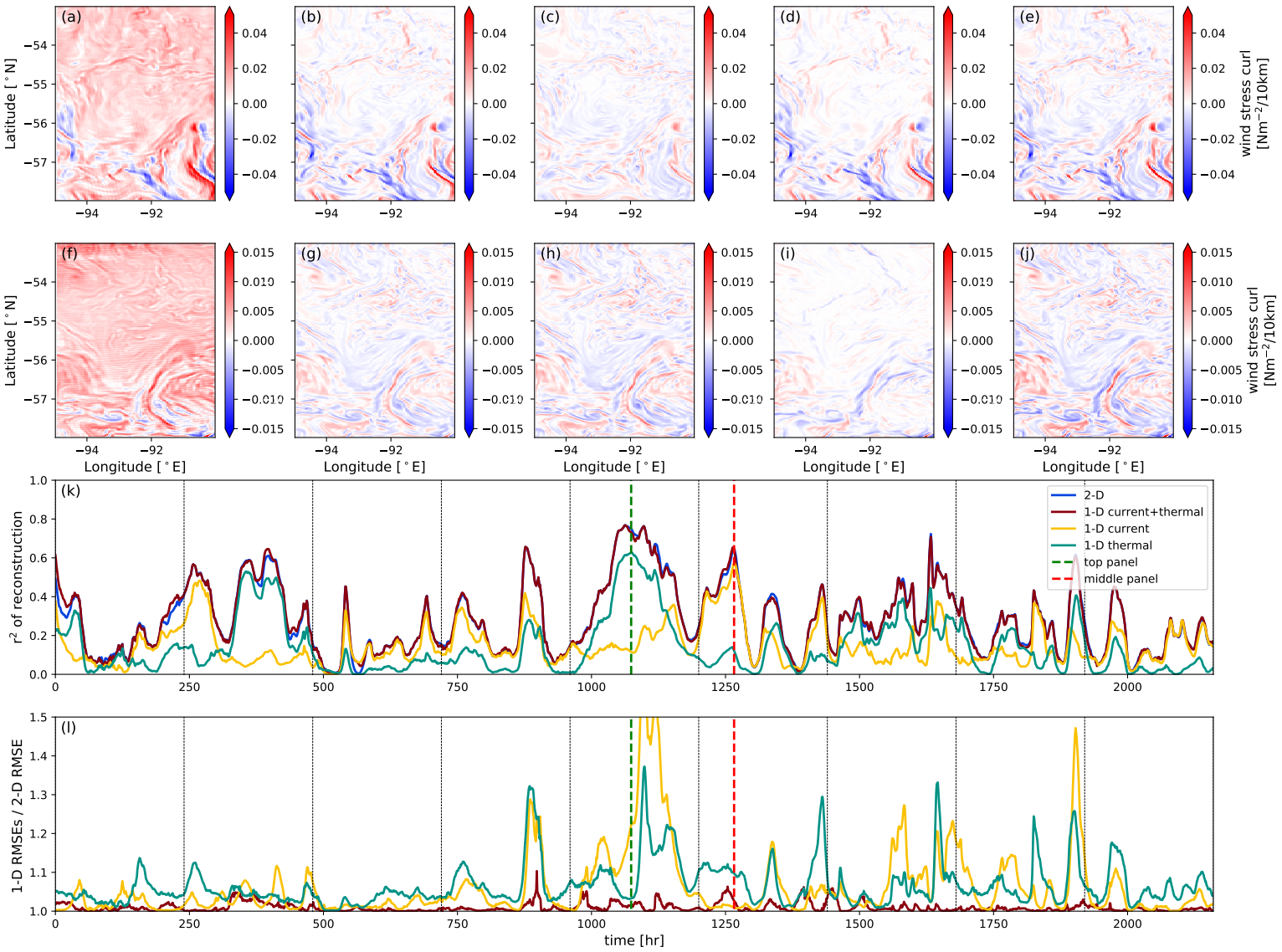

Figure S8. Same as in Fig. 3, but calculated in the quiescent subdomain (Fig. 1). Within the top two panels, from left to right are simulated wind stress curl (a,f), 2-D reconstruction (b,g), 1-D current reconstruction (c,h), 1-D thermal (d,i), and 1-D current + thermal (e,j).

subdomains, the essence of the 2-D conditional mean plot and our argument of the joint impact of wind-front interactions remain robust.

Specifically, tilted zero-lines, an indication of the constructive and destructive interactions between CFB and TFB, are seen in Fig. S7 a,d, even though the ranges of surface ocean vorticity/divergence and crosswind/downwind SST gradients in the quiescent regime are reduced by roughly a factor of 2. Therefore, wind stress curl reconstructions (Fig. S8) also require consideration of both the thermal and mechanical components. We again see alternating hourly reconstruction performances from 1-D current and 1-D thermal methods (Fig.S8 k,l), both of which retain ∼6% more RMSE on average than the 2-D dependent sum. The independent 1-D current + thermal reconstruction, on the other hand, only generates ∼1% more error, implying that in the quiescent region, CFB and TFB might be more independent than in the energetic subdomain. The correlation between the coefficients and physical parameters such as 10 m wind speed and air-sea temperature difference also remain and even strengthen, compared with the energetic region (Fig. S9). This suggests that α and β coefficients are more linearly correlated with physical parameters when Ro is smaller and the motions are dominated by larger scales.

Overall, the joint impact of current and thermal feedback applies in the quiescent region albeit with regional differences, as wind-front interactions are ubiquitous. More detailed spatial and temporal quantification of wind-front interactions are left for future work.

References

Balwada, D., Xiao, Q., Smith, S., Abernathey, R., & Gray, A. R. (2021). Vertical fluxes conditioned on vorticity and strain reveal submesoscale ventilation. *Journal of Physical Oceanography*, *51*(9), 2883–2901.

Farrar, J. T., D'Asaro, E., Rodriguez, E., Shcherbina, A., Czech, E., Matthias, P., ... Jenkins, R. (2020). S-mode: The sub-mesoscale ocean dynamics experiment. In *Igarss 2020-2020 ieee international geoscience and remote sensing symposium* (pp. 3533–3536).

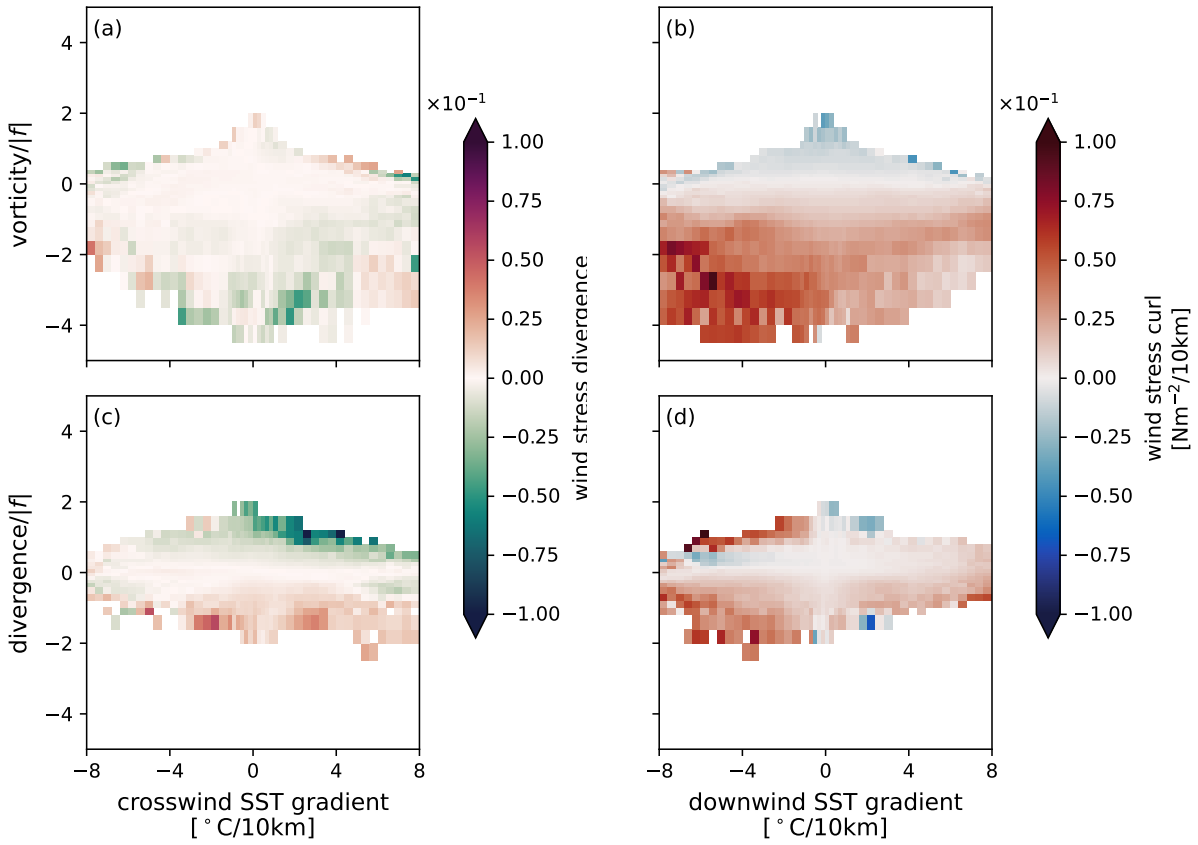

Figure S1. Conditional mean plots, for the combinations not presented in to Fig. 2. (a) Wind stress divergence is not correlated with ocean surface vorticity or crosswind SST gradient. (b) CFB from surface vorticity on wind stress curl. (c) CFB from surface divergence on wind stress divergence. (d) Wind stress curl is not correlated with surface divergence or downwind SST gradient.

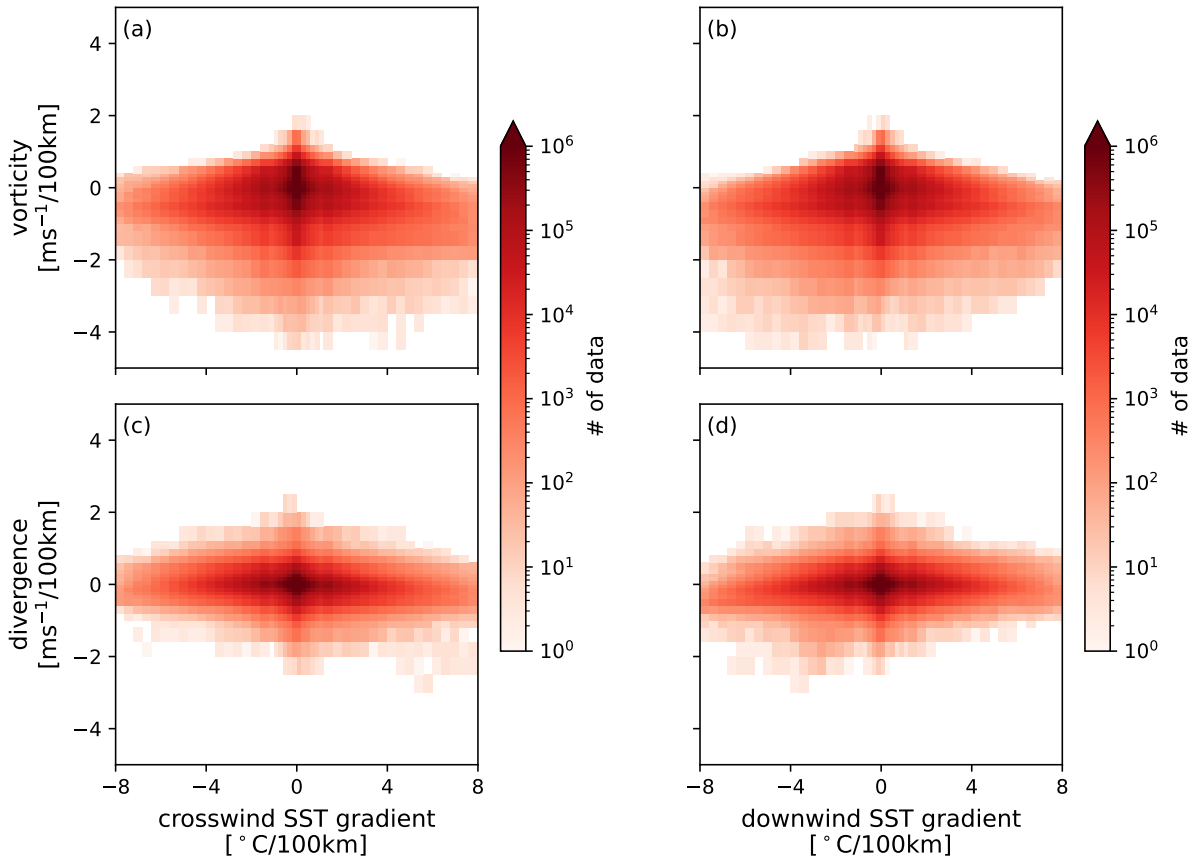

Figure S2. Total number of data within in ±1 standard deviation of the bin-averaged value. All panels are conditioned by the same physical properties as panels in Fig. 2 and Fig. S1.

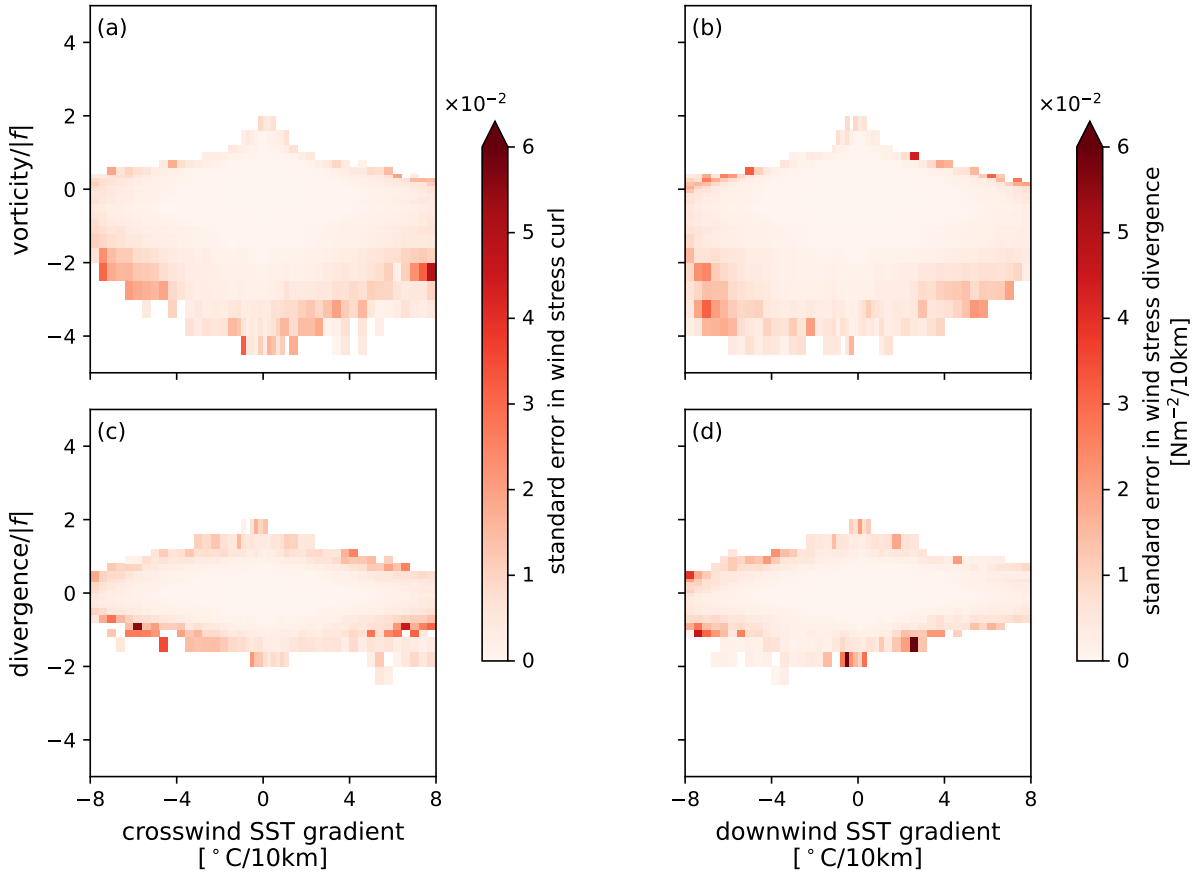

Figure S3. Standard error $\frac{\sigma}{\sqrt{n}}$ (σ is the standard deviation and n is the total number of points) in each bin. All panels are conditioned by the same physical properties as panels in Fig. 2 and Fig. S1, and therefore represent their standard error.

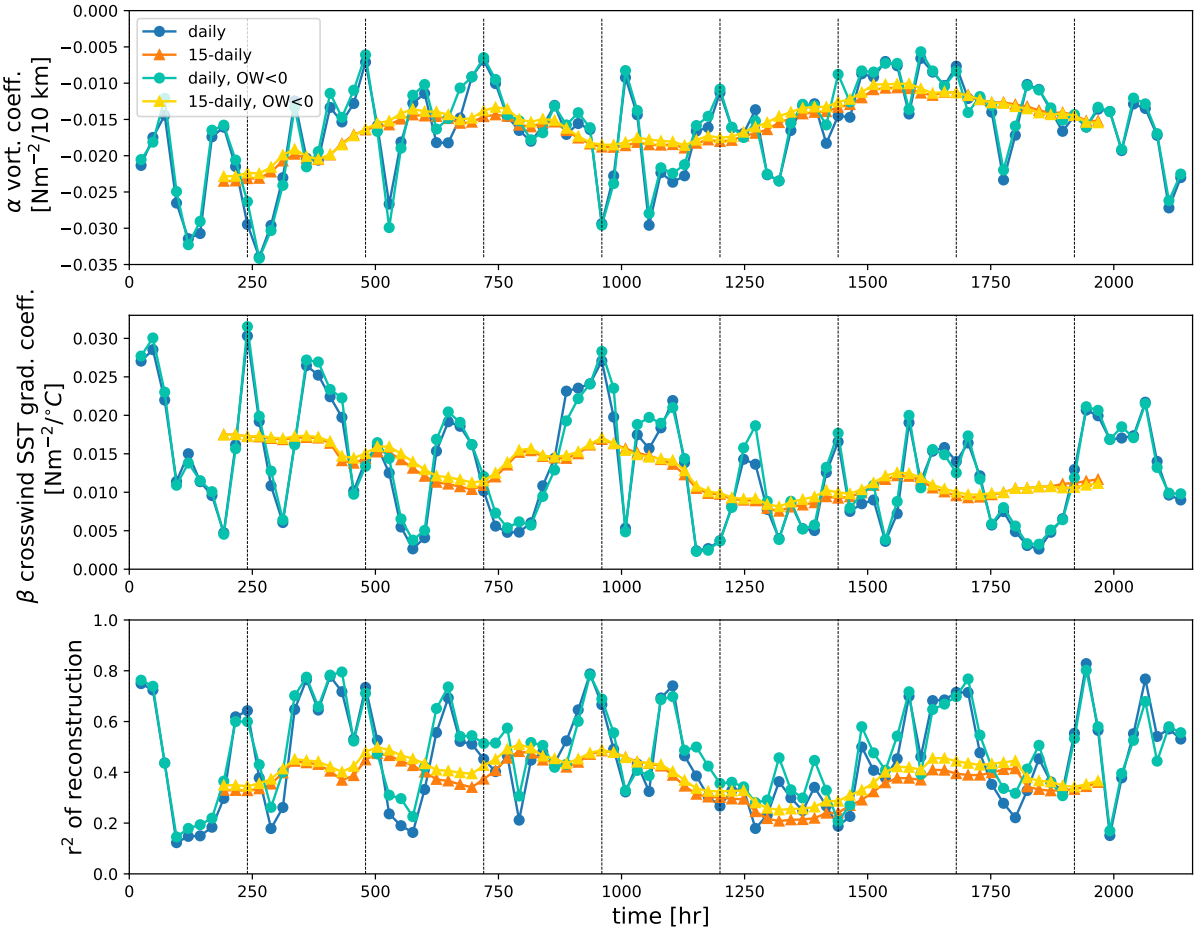

Figure S5. Wind-front feedback coefficients (Fig. 4) and 2-D reconstruction accuracy (Fig. 3) calculations, conditioned on Okubo-Weiss parameter in vorticity dominated regime. (a) Comparison of subdomain-based and $OW/f^2 < 0$ conditioned α calculations in one- and fifteen-day time windows. (b) β calculated as in (a). (c) Pearson linear correlation coefficients squared (r^2) of the 2-D reconstruction calculated with the same conditions and in the same time windows.

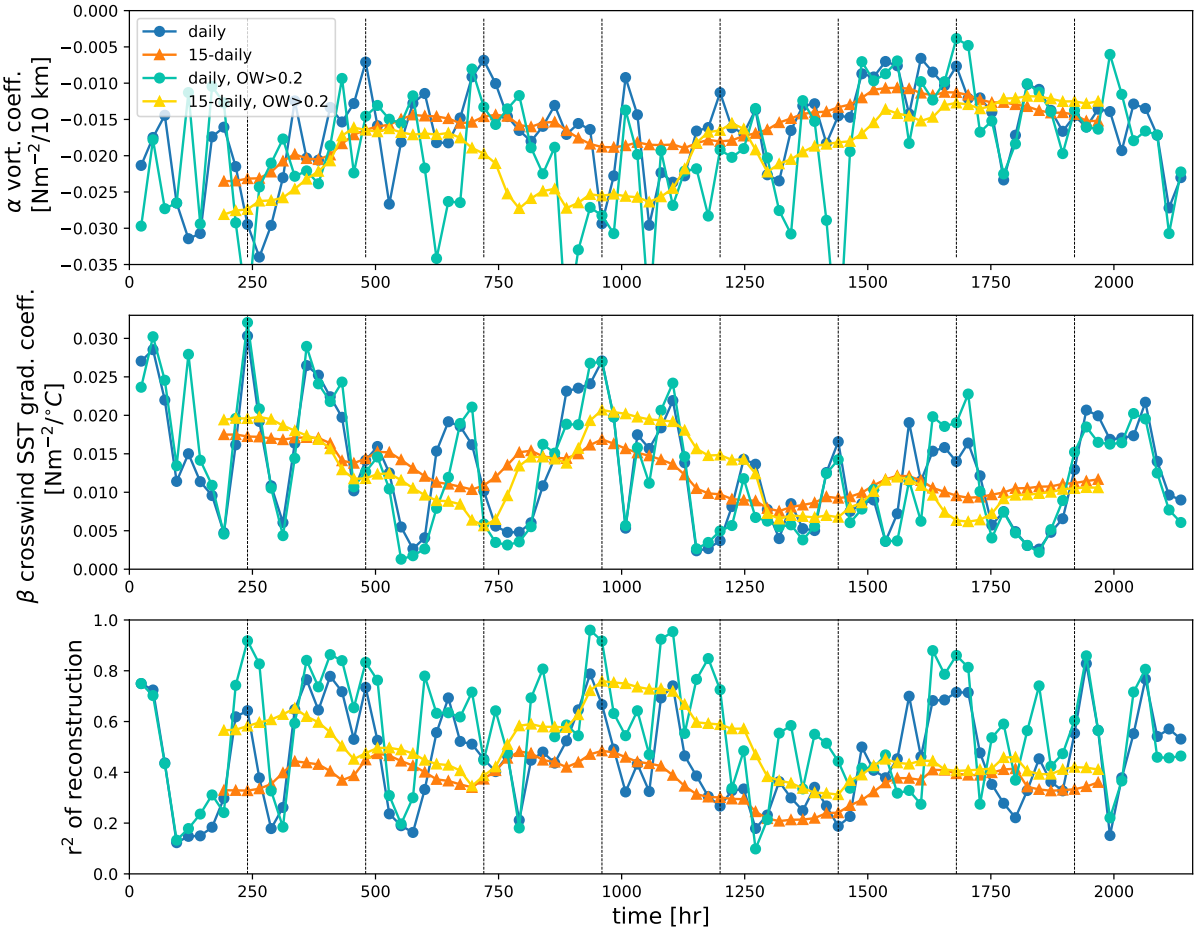

Figure S6. Same as in Fig. S5, but conditioned on Okubo-Weiss parameter in strain dominated regime, with $OW/f^2 > 0.2$.

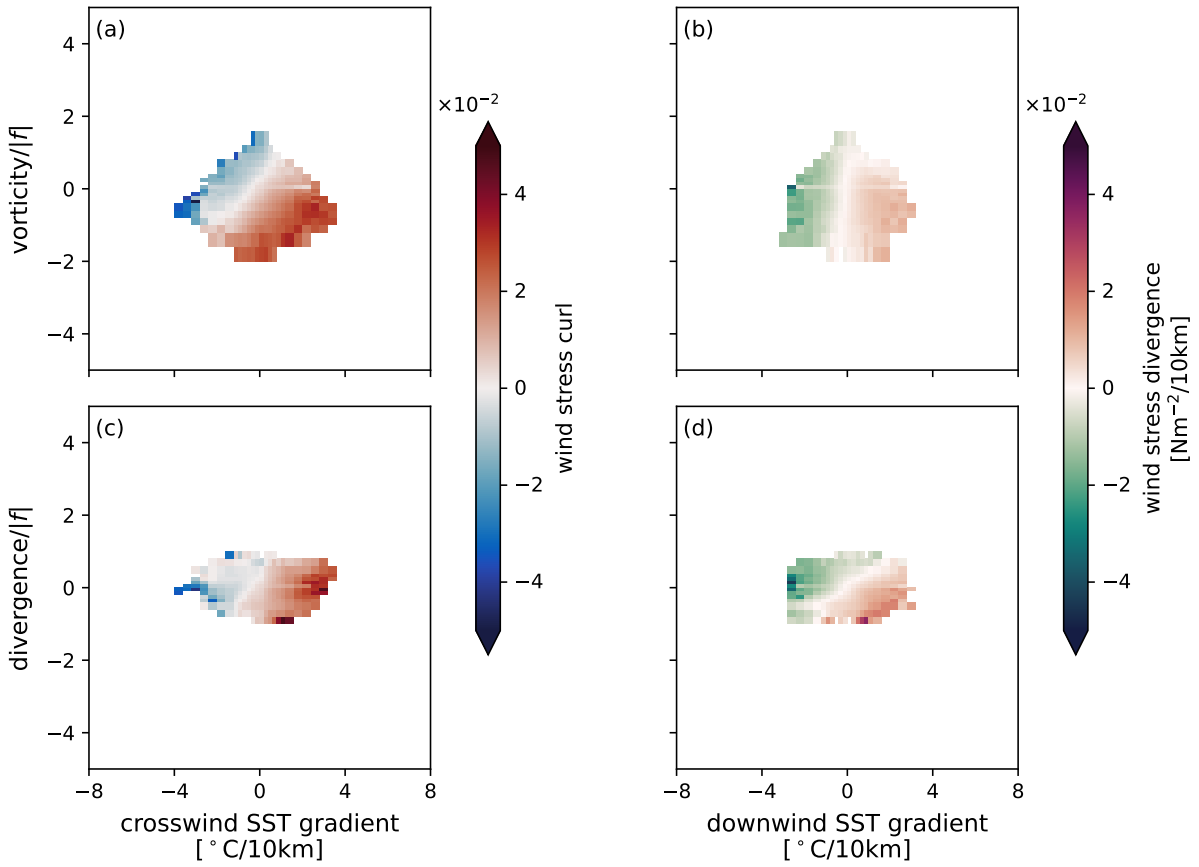

Figure S7. (quiescent subdomain) Conditional mean plots conditioned on surface ocean vorticity or divergence and crosswind or downwind SST gradients, colored by mean values of either wind stress curl or wind stress divergence. (a) The joint influence of vorticity and crosswind SST gradient on wind stress curl. (b) TFB from downwind SST gradient on wind stress divergence. (c) TFB from crosswind SST gradient on wind stress curl. (d) The joint influence of ocean divergence and downwind SST gradient on wind stress divergence. The slope of the zero-line (white in both colormaps) indicates the level of interaction and competition between surface vorticity/divergence and crosswind/downwind SST gradients in generating small-scale features in the wind stress fields.

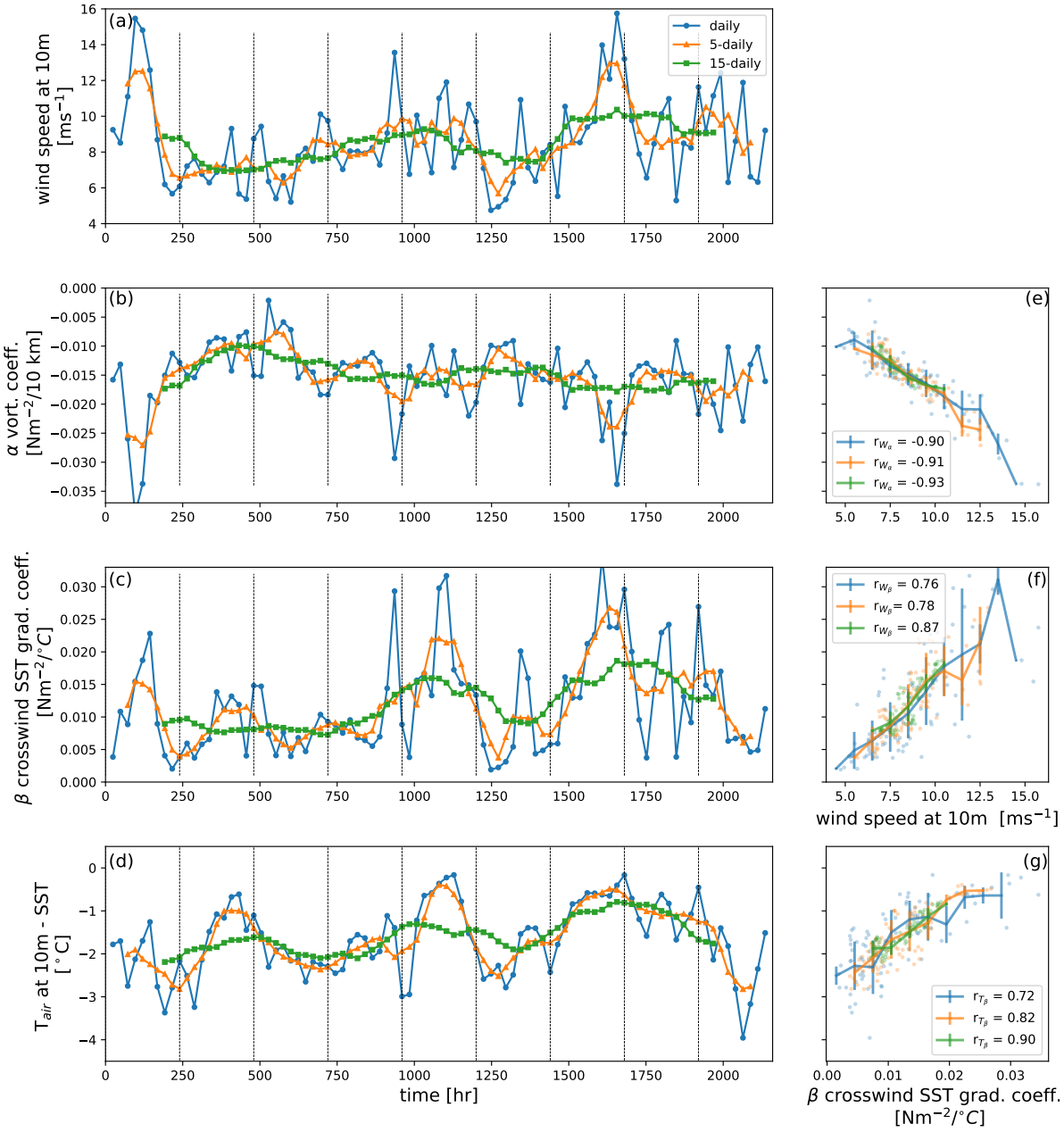

Figure S9. Variability and correlation of coefficients, α and β, and related physical properties, wind speed and air-sea temperature difference. (b) α; (c) β. (a) Wind speed and (d) air-sea temperature difference (air temperature at 10 m − SST) temporal variability are spatially averaged over the domain and over the same time period in which α and β are obtained. (e) correlation between wind speed and α with Pearson correlation coefficient r_{W_α}. (f) correlation between wind speed and β with Pearson correlation coefficient r_{W_β}. (g) correlation between air-sea temperature difference and β with Pearson correlation coefficient r_{T_β}.